Data-driven modeling of high-speed centrifugal compressors for aircraft Environmental Control Systems
Modélisation fondée sur des données de compresseurs centrifuges à grande vitesse pour les systèmes de contrôle de l'environnement des avions

Giuffré, A.; Ascione, F.; de Servi, C.M.; Pini, M.

Citation (APA)
Giuffré, A., Ascione, F., de Servi, C. M., & Pini, M. (2023). Data-driven modeling of high-speed centrifugal compressors for aircraft Environmental Control Systems: Modélisation fondée sur des données de compresseurs centrifuges à grande vitesse pour les systèmes de contrôle de l'environnement des avions. *International Journal of Refrigeration*, *151*, 354-369. https://doi.org/10.1016/j.ijrefrig.2023.03.019
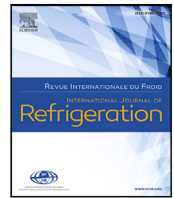
Important note
To cite this publication, please use the final published version (if applicable).
Please check the document version above.

Data-driven modeling of high-speed centrifugal compressors for aircraft Environmental Control Systems

Modélisation fondée sur des données de compresseurs centrifuges à grande vitesse pour les systèmes de contrôle de l'environnement des avions

Andrea Giuffre' [a], Federica Ascione [a], Carlo De Servi [a,b], Matteo Pini [a,*]

[a] *Propulsion and Power, Delft University of Technology, Kluyverweg 1, Delft, 2629HS, The Netherlands*
[b] *Energy Technology Unit, VITO, Beretang 200, 2400, Mol, Belgium*

ABSTRACT

The Environmental Control System (ECS) is the main consumer of non-propulsive power onboard aircraft. The use of an electrically-driven Vapor Compression Cycle (VCC) system, in place of the conventional air cycle machine, can lead to a substantial increase of the coefficient of performance. This work documents the development of an integrated design optimization method for VCC-based aircraft ECS, where the sizing of the system is performed along with the conceptual design of the compact heat exchangers and the high-speed centrifugal compressor. A data-driven model of the compressor has been developed to reduce the complexity of the VCC system model and the computational cost of the associated optimization problem. The model is based on artificial neural networks and has been trained on a synthetic dataset of 165k centrifugal compressor designs, generated with an in-house tool. The case study selected to demonstrate the capabilities of the proposed methodology is the multi-objective design optimization of an electrically-driven VCC system for the ECS of a single-aisle, short-haul aircraft, flying at cruise conditions. The results show that the number of function evaluations needed to identify the Pareto front reduces by a factor of three when using the data-driven model, in place of a meanline method. At the same time, the robustness of the numerical solver is improved, leading to the identification of optimal solutions covering a wider design space. Finally, the proposed methodology enables the analysis of the trends established between the system performance metrics and the design of the individual components.

1. Introduction

The continuous reduction of aircraft fuel consumption and emissions is a critical target for the aviation sector for economic, environmental, and societal reasons. To this purpose, the Advisory Council for Aeronautics Research in Europe (ACARE) is calling for innovative and sustainable technological solutions, to be implemented in the context of the More Electric Aircraft (MEA). The goals set by Europe with the Flightpath 2050 require a significant reduction of CO_2, NO_x, and noise emissions (ACARE, 2017). To reach these targets, a large number of resources have been invested in R&D programs for the development of new technologies for future aircraft, including the investigation of alternative concepts for non-propulsive aircraft subsystems. Among all the auxiliary subsystems, the Environmental Control System (ECS) is the largest consumer of non-propulsive power, accounting for up to 3%–5% of the total fuel burn (Bender, 2018). The ECS is responsible

for providing dry, sterile, and dust-free conditioned air to the airplane cabin at the proper temperature, flow rate, and pressure, to satisfy the safety and comfort requirements, as well as to ensure adequate avionics cooling (Dechow and Nurcombe, 2005). To reduce the fuel consumption of the ECS, the Boeing 787 has been equipped with a bleedless ECS, driven by an electrical motor. This solution eliminates the extraction of pneumatic power generated by the engines, and enables a reduction of specific fuel consumption in the range of 1%–2% at cruise conditions (Boeing, 2007). Furthermore, the replacement of the traditional Air Cycle Machine (ACM), i.e., an inverse Brayton cycle, with an electrically-driven Vapor Compression Cycle (VCC) system, can lead to a substantial increase of the Coefficient Of Performance (COP). Moreover, the adoption of an electrically-powered ECS is expected to reduce maintenance costs and increase system reliability, due to the removal of the maintenance-intensive bleed system. On the other hand,

---

Nomenclature

Roman symbols

$\dot{m}$	Mass flow rate [kg s^{-1}]
$\dot{Q}$	Heat flow rate [W]
$\dot{V}$	Volumetric flow rate [m^3 s^{-1}]
$\dot{W}$	Power [W]
$\hat{Y}$	Vector of model predictions [–]
A	Surface area [m^2]
b	Fins height [m]
C_r	Heat capacity ratio [–]
c_p	Specific heat capacity at constant pressure [J kg$^{(-1)}$ K$^{(-1)}$]
D	Diameter [m]
f	Friction factor [–]
F_{ax}	Axial thrust [N]
F_d	Flow depth [m]
F_p	Fins pitch [m]
G	Mass flux [kg m^{-2} s^{-1}]
g	Gravitational acceleration [m s$^{(-2)}$]
H	Blade height [m]
h	Specific enthalpy [J kg^{-1}] - Heat transfer coefficient [W m^{-2} K^{-1}]
j	Colburn factor [–]
k	Impeller shape factor [–] - Thermal conductivity [W m^{-1} K^{-1}]
k	Impeller shape factor [–]
L	Loss function [–]
L/D	Lift to drag ratio [–]
l_f	Fin length [m]
L_h	Louver height [m]
L_l	Louver length [m]
L_p	Louver pitch [m]
l_t	Tube length [m]
Ma	Mach number [–]
N	Fluid molecular complexity [–] - Number of items [–]
n	Number of samples [–]
Nu	Nusselt number [–]
OR	Operating range [–]
P	Pressure [Pa]
P_t	Tubes pitch [m]
Pr	Prandtl number [–]
R	Radius [m] - Thermal resistance [K W^{-1}]
Ra	Surface roughness [m]
Re	Reynolds number [–]
SFC_P	Power specific fuel consumption [lb hp$^{(-1)}$ h$^{(-1)}$]
SFC_{th}	Thrust specific fuel consumption [lb lbf$^{(-1)}$ h$^{(-1)}$]
T	Temperature [K]
t	Thickness [m]
T_h	Tube height [m]
U	Peripheral speed [m s^{-1}] - Overall heat transfer coefficient [W m^{-2} K^{-1}]
u	Flow velocity [m s^{-1}]
V	Absolute velocity [m s^{-1}] - Volume [m^3]
v_{air}	Airspeed [m s$^{(-1)}$]
W	Relative velocity [m s^{-1}]
W_{ECS}	ECS pack weight [kg]
W_{f0}	Fuel weight penalty [kg]
x	Vapor quality [–] - Width [m]
Y	Vector of true labels [–]
y	Height [m]
z	Depth [m]
NTU	Number of Transfer Units [–]

Greek symbols

α	Absolute flow angle [°]
β	Pressure ratio [–]
$\boldsymbol{\alpha}$	Vector of design variables [–]
$\boldsymbol{\theta}$	Vector of hyperparameters [–]
δ	Thickness [m]
ϵ	Effectiveness [–]
ϵ_b	Back face clearance [m]
ϵ_t	Tip clearance gap [m]
η	Efficiency [–]
η_c	Fin surface effectiveness [–]
η_f	Fin efficiency [–]
γ_{Pv}	Isentropic pressure–volume exponent [–]
ν	Poisson's ratio [–]
Ω	Rotational speed [rpm]
Φ_{t1}	Swallowing capacity [–]
Ψ_{is}	Isentropic loading coefficient [–]
ρ	Density [kg m^{-3}]
τ	Aircraft mission time [h]
Θ	Louver angle [°]

Subscripts

1	Impeller inlet
2	Impeller outlet
3	Diffuser outlet
4	Volute outlet
air	Air stream
bl	Blade
CC	Cabin Compressor
cond	Condensation

the VCC system may not meet the requirements of high cooling power and low air temperature at the discharge of the ECS pack, occurring when the system operates on ground at high ambient temperature and high relative humidity. To overcome this limitation, Airbus and Liebherr are jointly developing a novel electrically-driven ECS concept based on a hybrid architecture, which integrates an ACM and a VCC system (Schmidt et al., 2021). A similar concept has been investigated also by DLR (Bender, 2018). Fig. 1 shows the simplified process flow diagram of the three mentioned ECS architectures.

A thorough attempt to derive an analytical formulation for the COP of aircraft ECS, based on the ACM technology, can be found in Yang and Yang (2020b). Using the endoreversible thermodynamic analysis, the authors obtained an explicit formulation of the COP for five different ACM configurations. However, the derivation presented in the paper is based on the assumption of dry air and ideal gas, thus it is not directly applicable to VCC systems, where the working fluid experiences phase changes, and does not obey the ideal gas law. Moreover, in the aforementioned study, the authors did not account for the conceptual design of the main components of the ECS, namely, the heat exchangers and the turbomachinery. However, as reported by the same authors in Yang and Yang (2020a), the performance of the

des	Desuperheating
el	Electrical
eva	Evaporation
ext	External
f	Fin
h	Hub
hyd	Hydraulic
is	Isentropic
mc	Microchannel
refr	Refrigerant stream
sub	Subcooling
t	Tube
ts	Total-to-static
tt	Total-to-total

Abbreviations

ACM	Air Cycle Machine
ANN	Artificial Neural Network
CHEX	Compact Heat Exchanger
CO_2	Carbon Dioxide
con	Constraints
COP	Coefficient Of Performance
ECS	Environmental Control System
FV	Finite Volume
H_2	Hydrogen
HEX	Heat Exchanger
mae	Mean absolute error
mape	Mean absolute percentage error
MB	Moving Boundary
MLP	Multi-Layer Perceptron
obj	Objectives
pp	Pinch point
R-1233zd(E)	Trifluoropropene
R-134a	Tetrafluoroethane
sc	Subcooling
sh	Superheating
VCC	Vapor Compression Cycle

ECS is highly affected by the design of its components. Therefore, the optimal design of the system can be arguably achieved only by resorting to an integrated design approach, i.e., a framework in which the design variables of the system and those related to the preliminary design of the main components are optimized simultaneously. A pioneering application of the integrated design method for the optimization of a simplified ECS configuration is documented in Vargas and Bejan (2001). Following this work, numerous attempts have been made to apply the integrated design approach to more complex and more realistic ECS configurations. In Pérez-Grande and Leo (2002), the authors performed a multi-objective optimization of a two-wheel bootstrap ACM, including the design of the two offset strip fin heat exchangers. The objectives selected for the optimization were the minimization of the volume of the heat exchangers, and the minimization of the total entropy generation at cruise. The study has been subsequently extended to include a thermoeconomic analysis, as documented in Leo and Pérez-Grande (2005). More recently, an unconventional ECS architecture, featuring a hybrid ACM-VCC system, has been targeted for a multi-objective optimization (Sielemann et al., 2011). In this work, the ECS has been simulated under three different operating conditions, and the specific fuel consumption (SFC) has been computed as a weighted average of the values obtained in the three scenarios. An alternative strategy

to compute the thermodynamic characteristics of a conventional ECS configuration has been proposed by Li et al. (2019). By adopting the heat current method, in place of the energy flow method, the authors were able to reduce the number of independent variables and governing equations of the system, thus simplifying its solution for analysis and optimization purposes. In Duan et al. (2022), the authors performed a multi-objective optimization of a three-wheel bootstrap ACM, including the high-pressure water separation loop. The optimization featured four design variables, namely, the effectiveness of the four heat exchangers, two objectives, i.e., the entropy generation rate and the number of transfer units (NTU) of the ECS, and five non-linear constraints.

All the aforementioned studies have targeted conventional or hybrid ACM configurations, focusing the modeling effort on the heat exchangers. However, in a VCC system featuring a high-speed centrifugal compressor operating with gas bearings, the most critical component of the system is arguably the compressor. Indeed, the operating range of the VCC system is limited by the choke and stall margins of the compressor, and the COP is highly affected by the efficiency of the turbomachine. Therefore, in order to perform an integrated design optimization of a VCC system, it is necessary to include a conceptual design model of the turbo-compressor. However, this further complicates the mathematical problem associated with the ECS model and increases the number of design variables and non-linear constraints to be included in the optimization. As a result, the robustness of the numerical solver decreases, due to the higher likelihood of an ill-conditioned matrix, and the computational cost of the optimization problem quickly becomes prohibitive, even for relatively simple ECS configurations. In light of the above, the availability of a strategy to reduce the complexity of the system model, without sacrificing the accuracy of the solution, assumes paramount importance.

2. Objective

The objective of the present study is to bridge the knowledge gap regarding the integrated design of VCC-based ECS systems, including the conceptual design of high-speed centrifugal compressors. This target is achieved through two intermediate steps. First, a methodology to derive a data-driven model for high-speed centrifugal compressors is proposed. Second, the capabilities of an optimization methodology, exploiting this data-driven model for the integrated design of novel VCC-based ECS, are demonstrated.

The paper is structured as follows. First, the models of the main components of the ECS are introduced, highlighting the main sources of complexity for system simulations. Then, the integrated design methodology is described and the problem of computational cost is discussed. Next, the data-driven compressor model is developed and coupled to the optimization framework, to reduce the computational overhead associated with the compressor model, while retaining engineering accuracy. A multi-objective design optimization of the electrically-powered ECS is performed at cruise conditions with two different methodologies: a conventional one, where the compressor preliminary design is addressed by means of a meanline code, and the proposed one, in which the meanline code is replaced with the data-driven model. The results are compared in terms of optimal solutions and computational cost. Moreover, a sensitivity analysis is performed to assess the robustness of the optimal solutions to changes in the values of the design variables and to identify the design variables which mostly affect the objective functions. Finally, concluding remarks summarize the lessons learnt and provide an outlook for future work.

3. Methodology

The present work deals with the multi-objective optimization of an ECS for a single-aisle, short-haul aircraft, e.g., the Airbus A320. One ECS architecture and one operating condition are considered:
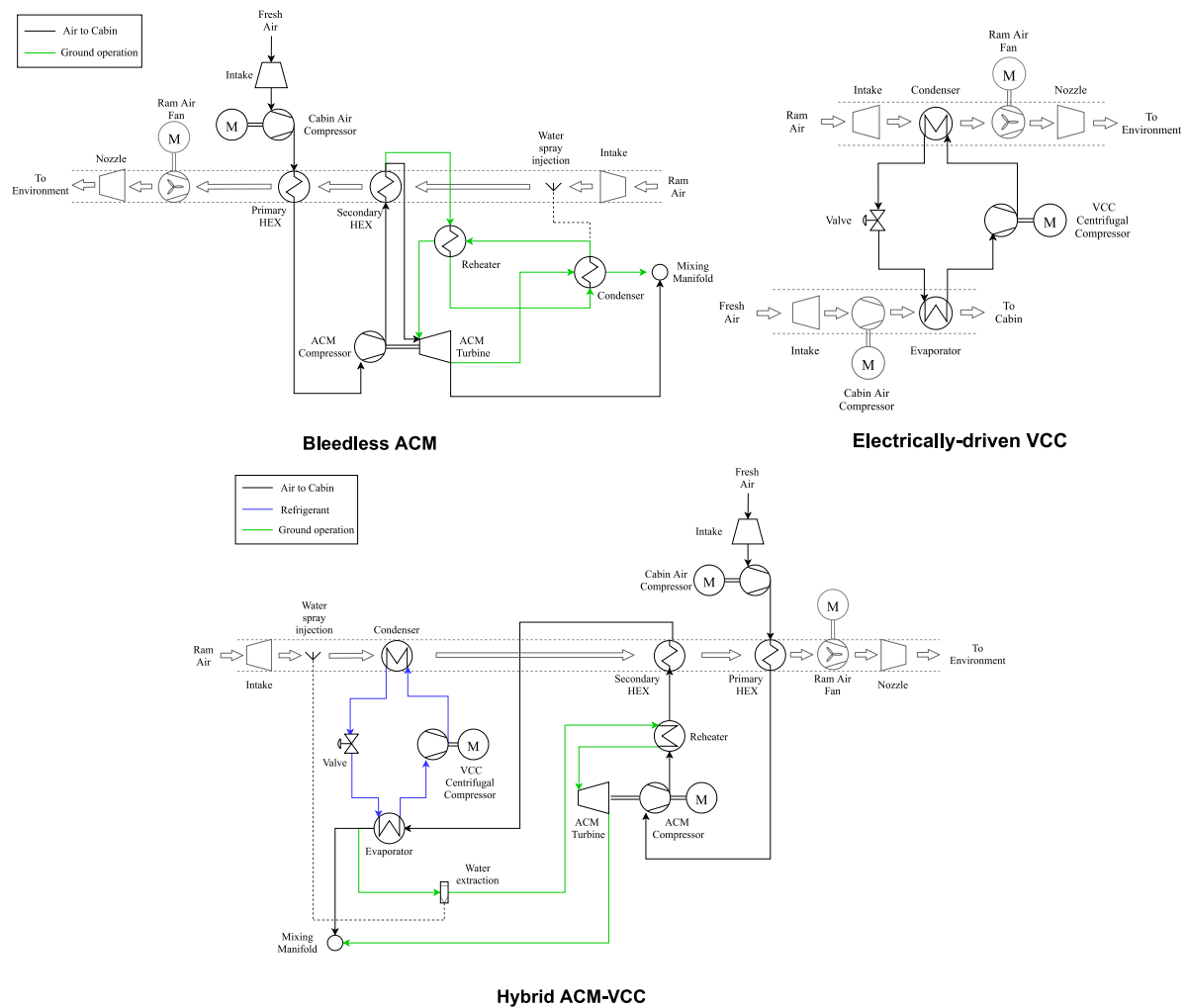
Fig. 1. Simplified process flow diagram of three novel environmental control system architectures.

a single-pressure level, electrically-driven VCC system, operating at cruise, under mild cooling requirements.

The main components of the selected VCC system are: two compact heat exchangers (CHEXs), an expansion valve, and a high-speed centrifugal compressor operating with gas bearings. The use of a turbo-compressor, in place of a conventional scroll compressor, enables an increase of the system COP, while reducing its volume and weight. The COP of the VCC system can be further enhanced by adopting a configuration featuring multiple pressure levels. However, this is beyond the scope of the present work.

The ECS based on the electrically-driven VCC technology has been modeled by resorting to the acasual (Schweiger et al., 2020), object-oriented, equation-based Modelica language, see Fig. 2. The additional components needed to simulate the performance of the VCC-based ECS are: two intakes for the ram air and the cabin air, respectively, the cabin air compressor, the ram air fan, and the nozzle, used to accelerate the ram airflow at the exhaust. All the components are steady-state, zero-dimensional, except for the compressor, which features a mean-line model. The refrigerant selected for the application is the R-134a, i.e., the standard working fluid used for VCC-based ECS, such as those of helicopters.

3.1. Heat exchangers

The VCC system features two CHEXs: the condenser and the evaporator. The prescribed topology is the one commonly adopted in automotive applications, namely, a bundle of flat tubes with an internal microchannel structure, and louver fins on the external surface, as displayed in Fig. 3. This topology allows for a large heat transfer surface on the air stream side, thus enhancing the heat transfer efficiency, without increasing the total volume occupied by the heat exchanger. The fins and tube geometries have been modeled following the guidelines provided in Shah and Sekulić (2003). The air and the refrigerant flow into the fins and the flat tubes, respectively, according to an unmixed cross-flow arrangement. The refrigerant undergoes a phase change along the CHEXs tubes. To capture this phenomenon, the model of these devices features a number of control volumes equal to the number of phases undertaken by the refrigerant during the thermodynamic process. For instance, the condenser is divided into three sections: desuperheating (superheated vapor), condensation (two-phase flow), and subcooling (liquid phase), as displayed in Fig. 4. This modeling approach, known as Moving Boundary (MB) method, has been selected in place of the Finite Volume (FV) method, since it guarantees a better trade-off between model complexity and accuracy, as demonstrated by Pangborn et al. (2015).

By adopting the MB method, it is possible to estimate the heat transfer coefficient and the pressure drop occurring in the CHEX using the most appropriate correlations for each refrigerant phase. These equations are based on non-dimensional numbers, i.e., the Colburn factor j and the Nusselt number Nu for the heat transfer coefficient, and the friction factor f for the pressure drop. The Colburn factor j of the air passing through the multi-louvered fins is retrieved using the correlation by Chang and Wang (1997), and the corresponding heat
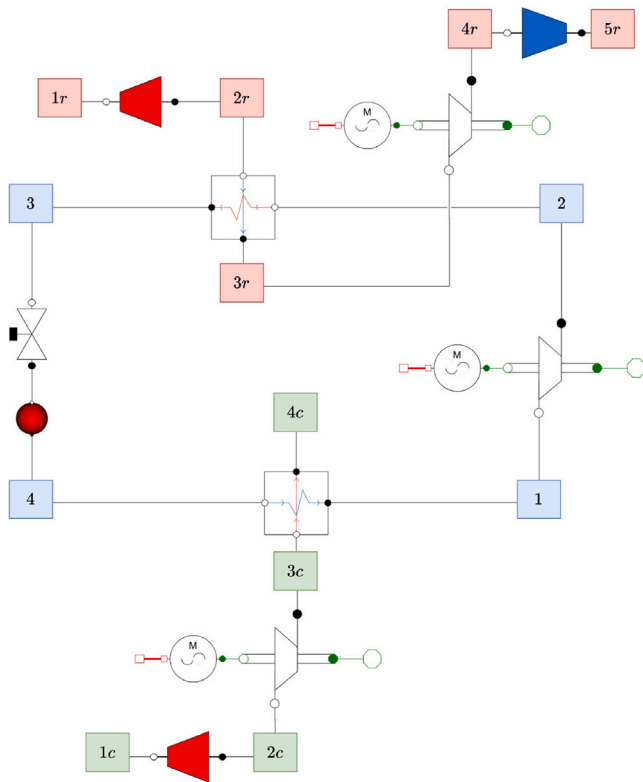
Fig. 2. Modelica model of the electrically-driven VCC system. The thermodynamic states are highlighted as follows: ram air stream in red, cabin air stream in green, and refrigerant loop in blue. (For interpretation of the references to color in this figure legend, the reader is referred to the web version of this article.)
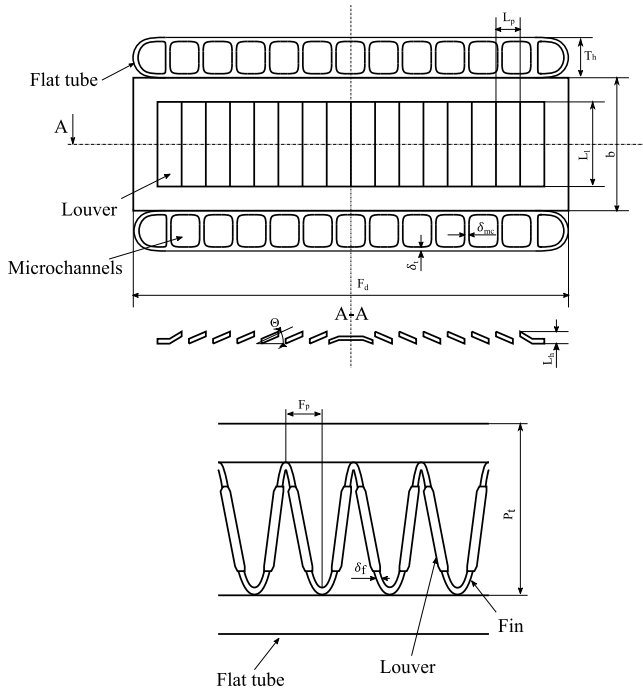

Fig. 3. Internal geometry of a heat exchanger featuring multi-louvered fins and flat tubes with microchannels.

transfer coefficient computed as
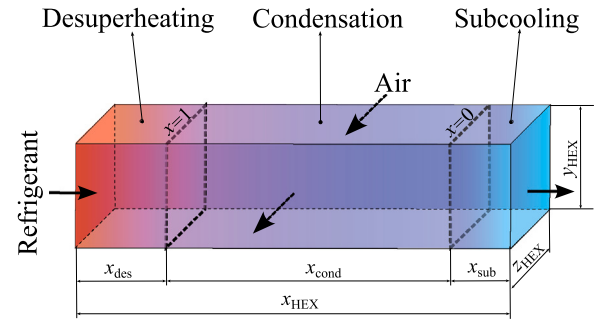
$$h = j \frac{c_p G}{Pr^{2/3}}. \tag{1}$$

Fig. 4. Schematic of the condenser model based on the Moving Boundary approach. The fluid vapor quality x determines the subdivision among the different phases.

The heat transfer coefficient of the single-phase refrigerant flow is computed as a function of the Nusselt number estimated with the correlation by Gnielinski (2013)

$$h = Nu \frac{k}{D_{\mathrm{hyd}}}. \tag{2}$$

In the case of condensing and evaporating refrigerant flow, the heat transfer coefficient is determined according to Shah (1979) and Kandlikar (1990), respectively. The heat transfer rate is estimated using the $\epsilon - NTU$ method, where the definition of ϵ depends on both the flow arrangement and the phase of the refrigerant (Kim and Bullard, 2002a). In case of unmixed cross-flow and single-phase flow, it is expressed as

$$\epsilon = 1 - \exp\left\{ \frac{NTU^{0.22}}{C_\mathrm{r}} \left[\exp\left(-C_\mathrm{r} NTU^{0.78} \right) - 1 \right] \right\}. \tag{3}$$

On the opposite, if evaporation or condensation occurs within the heat exchanger tubes, the heat capacity ratio C_r is null, and the effectiveness can be simply expressed as

$$\epsilon = 1 - e^{-NTU}. \tag{4}$$

The NTU is defined as the product of the overall heat transfer coefficient U and the total heat transfer surface A, divided by the minimum heat transfer capacity between the two working fluids. The overall heat transfer coefficient UA accounts for both the effect of convection and of conduction, due to the presence of the fins and the tubes

$$\frac{1}{UA} = \frac{1}{h_{\mathrm{air}} \eta_\mathrm{c} A_{\mathrm{air}}} + \frac{1}{h_{\mathrm{refr}} A_{\mathrm{refr}}} + R_\mathrm{t}. \tag{5}$$

The fins surface effectiveness η_c is a function of the fin efficiency η_f (Kim and Bullard, 2002a)

$$\eta_c = 1 - \frac{A_\mathrm{f}}{A_{\mathrm{air}}} \left(1 - \eta_\mathrm{f} \right) = 1 - \frac{A_\mathrm{f}}{A_{\mathrm{air}}} \left(1 - \frac{\tanh m l_\mathrm{f}}{m l_\mathrm{f}} \right), \tag{6}$$

where

$$m = \sqrt{\frac{2 h_{\mathrm{air}}}{k_\mathrm{f} \delta_\mathrm{f}} \left(1 + \frac{\delta_\mathrm{f}}{F_\mathrm{d}} \right)}, \tag{7}$$

$$l_\mathrm{f} = \frac{H}{2} - \delta_\mathrm{f}. \tag{8}$$

The thermal resistance of the microchannel walls is estimated as (Yadav et al., 2017)

$$R_\mathrm{t} = \frac{1}{2\pi k} \left(\frac{1}{l_\mathrm{t} N_{\mathrm{mc}} N_\mathrm{t}} \right) \log\left(\frac{D_{\mathrm{ext,mc}}}{D_{\mathrm{ext,mc}} - 2\delta_{\mathrm{mc}}} \right). \tag{9}$$

The pressure losses due to friction depend on both the fluid phase and the heat exchanger geometry. In the present work, the friction coefficient f of the airflow is computed using the correlation proposed by Kim and Bullard (2002a). For what regards the refrigerant stream, the model proposed by Schmidt and Friedel (1997) has been selected as the most suitable for the case of two-phase flow. A well-established

set of correlations for pressure drops in straight tubes has been implemented to model pressure drops for single-phase flow, depending on the Reynolds number. The complete list of references is reported in Ascione et al. (2021). Finally, once the tube geometry and the fluid mass flow rate are fixed, the total pressure drop can be calculated as

$$\Delta P = f \frac{l_t}{D_{hyd}} \frac{\rho u^2}{2}. \tag{10}$$

All the correlations used in this work have been verified using experimental data available in the literature, and the results are reported in Table 1. Moreover, the condenser model has been validated against the experimental data published by Kim and Bullard (2002b). The results show a 10% discrepancy in the estimation of the pressure drop and a deviation lower than 4% in the calculation of the available heat transfer surface. No comparison has been performed in terms of heat transfer coefficient since no experimental data for this quantity are available in the aforementioned study.

The heat exchanger models include also a method to estimate the dry weight of the device. Once the geometry has been fully determined, the volume of the material forming the HEX core can be computed as the sum of the volume occupied by the fins V_f, and that of the microchannels tubes V_t. With reference to Fig. 3, these two volumes can be expressed as

$$V_f = \delta_f \left[\left(b^2 + F_p^2 \right)^{1/2} - \delta_f \right] F_d N_f$$
$$V_t = x_{HEX} \left[\frac{\pi}{2} \delta_t N_t \left(T_h + F_d - 2\delta_t \right) + \delta_{mc} \left(T_h - 2\delta_t \right) \left(N_{mc} - 1 \right) \right]. \tag{11}$$

Then, based on the prescribed material, the weight of the heat exchanger is computed as the product of the material density and the total volume. Finally, the result is multiplied by an empirical coefficient, accounting for the presence of casing, manifold, and soldering.

3.2. Centrifugal compressor

A detailed description of the model developed in-house for the conceptual design of single-stage centrifugal compressors can be found in Giuffre et al. (2022). In this section, only the fundamental building blocks are reviewed, and emphasis is given to the simplifications adopted when implementing it in Modelica.

With reference to Fig. 5, the compressor sizing is performed on the basis of ten design variables, namely: the swallowing capacity

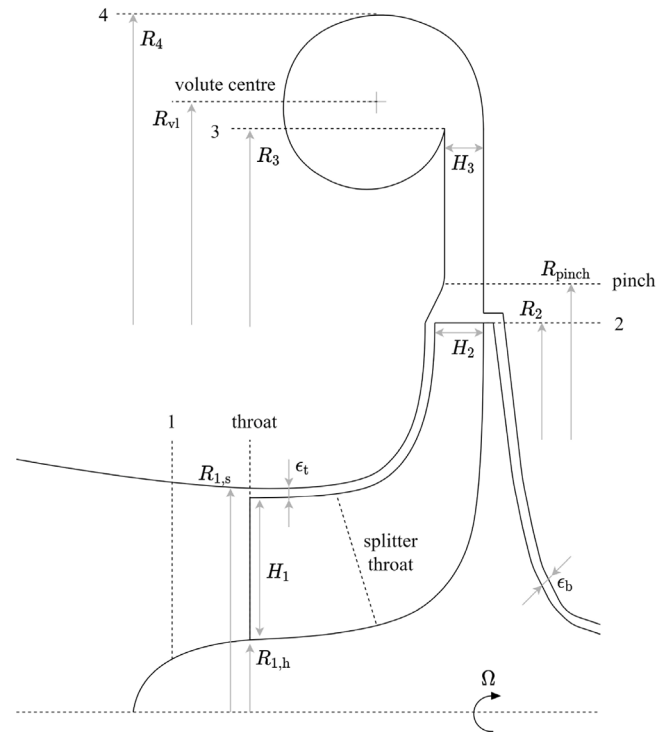$$\phi_{t1} = \frac{\dot{m}}{\rho_{t1} U_2 D_2^2}, \tag{12}$$

the isentropic loading coefficient

$$\psi_{is} = \frac{\Delta h_{tt,is}}{U_2^2}, \tag{13}$$

the impeller shape factor

$$k = 1 - \left(\frac{R_{1,h}}{R_{1,s}} \right)^2, \tag{14}$$

the total-to-total pressure ratio (β_{tt}), the mass flow rate $(\dot{m})$, the impeller outlet absolute flow angle (α_2), the number of blades (N_{bl}),

Fig. 5. Meridional view of a centrifugal compressor stage featuring splitter blades, pinched vaneless diffuser, overhung volute, and no inlet guide vanes.

the diffuser radius ratio (R_3/R_2), and the non-dimensional parameters characterizing the shape of the diffuser

$$R_{r,pinch} = \frac{R_{pinch} - R_2}{R_3 - R_2}$$
$$H_{r,pinch} = \frac{H_3 - H_2}{H_2(R_2/R_{pinch} - 1)}. \tag{15}$$

Moreover, the model requires the specification of the working fluid, the total inlet conditions, and a list of geometrical parameters related to manufacturing constraints, e.g., the impeller tip clearance gap.

The compressor design methodology is based on the lumped parameters modeling approach. However, the flow quantities are evaluated at five different spanwise locations at the inducer section, to account for the spanwise variation of the peripheral speed. The inlet velocity triangle is determined by the choice of ϕ_{t1} and by the minimization of the relative Mach number at the inducer shroud (Rusch and Casey, 2013). The first guess of the outlet velocity triangle is set by the selection of α_2 and ψ_{is}. The actual work coefficient is then iteratively adjusted to match the target pressure ratio, accounting for slip (von Backström, 2006) and losses, which are predicted by means of the set of semi-empirical correlations reported in Giuffre et al. (2022). The flow in the vaneless diffuser is modeled by integrating the system of two-dimensional differential equations derived by Stanitz (1952). The axial thrust acting on gas bearings is computed following the approach

devised by Tiainen et al. (2021). The model can be used both for designing a compressor stage, as well as for computing its operating map, once the main dimensions have been determined. However, for the sake of brevity, the prediction of the compressor off-design performance is not described here, and the interested reader is referred to Giuffre et al. (2022) for further information.

To assess the accuracy of the compressor model, the predictions of the in-house tool have been compared with the experimental data of three reference test cases available in literature (Eckardt, 1975, 1976, 1977; Japikse, 1987; Schiffmann and Favrat, 2009, 2010), and with the CFD simulation results of a new compressor prototype. As documented in Giuffre' et al. (2023), the outcome of the validation study is that more than 95% of the experimental and CFD data fall within the ±5% uncertainty bands of the values predicted by the model.

The main simplifications adopted when implementing the aforementioned compressor model in Modelica are: (i) the span-wise distribution of flow quantities at the inducer section is neglected, (ii) the flow in the vaneless diffuser is described with a simplified model (Amirante et al., 2015), which does not require any stream-wise discretization of the flow quantities; (iii) the compressor performance are computed only at design point. Despite these simplifications, when integrating the compressor design tool within the model of the VCC system, the non-linearity of the resulting system of equations increases remarkably, as well as the number of design variables. As stated in the introduction, this leads to a reduction of the robustness of the numerical solver, and to a substantial increment of the computational cost, when performing an integrated design optimization.

3.3. Data-driven compressor model

To reduce the complexity of the ECS model and the computational cost of the corresponding optimization problem, a data-driven compressor model has been developed and integrated into the existing design framework. Recently, a surrogate model for small-scale single-stage centrifugal compressors has been developed by Mounier et al. (2018). Using a symbolic regression tool, the authors obtained an analytical expression of the isentropic efficiency at the design point, as a function of five non-dimensional groups and the total inlet pressure. The data-driven regression has been performed on a dataset comprising approximately 12.5k compressor designs, obtained by means of a mean-line tool, validated with experimental data. However, the proposed reduced-order model has the following limitations. All the compressor stages featured in the dataset have been designed to operate with R-134a. Moreover, a number of geometrical parameters characterizing the shape and the performance of the compressor stage, e.g., the impeller outlet blade angle, have been set at constant values, or have been determined by prescribing a constant ratio among two geometrical parameters, e.g., the diffuser radius ratio. Therefore, the dataset is biased, and the resulting analytical expression of the efficiency is not applicable to a compressor stage operating with an arbitrary working fluid and featuring a generic shape. Furthermore, the proposed data-driven model does not provide any prediction of the operating range of the machine, thus it may lead to compressor configurations that are unfeasible for systems that require a broad operating envelope, such as the ECS of aircraft.

To overcome these limitations, a new methodology to derive a data-driven model for single-stage centrifugal compressors is proposed in this work. In the same fashion as in Mounier et al. (2018), the dataset has been generated with a validated compressor model (Giuffre et al., 2022). The synthetic dataset comprises 240k unique compressor stage designs, characterized by different combinations of the design variables listed in Table 2, and sampled according to the latin hypercube method. Differently from the aforementioned study, none of the main geometrical characteristics of the stage has been fixed to a constant value. Nevertheless, the number of design variables considered to create the dataset is relatively limited, thanks to the adoption of a non-dimensional approach based on scaling analysis. The additional compressor design parameters related to manufacturing constraints have been set to constant values, namely, $\epsilon_b = \epsilon_t = 0.15$ mm, $Ra = 3.2$ μm. Finally, to cope with the design of compressors of different sizes, the ratio between the shaft and the inlet hub radii has been fixed throughout the design space, instead of prescribing a constant value of shaft radius.

The working fluids considered in the present work are synthetic and natural refrigerants selected from a parametric study conducted for an electrically-driven VCC for the ECS of large helicopters (Ascione et al., 2021). To enrich the dataset, the compressor stages operating with the refrigerants R-134a and R-1233zd(E) have been designed for two different total inlet thermodynamic states, resembling the conditions encountered in a conventional and a high-temperature heat pump. To reduce bias in the dataset and extend the range of applicability of the data-driven compressor model, the database has been complemented with compressor stages designed for simpler molecule fluids, i.e., CO_2 and H_2. Additional working fluids and thermodynamic conditions will be included as part of future work. The complete list of fluids and of the corresponding reduced inlet conditions, i.e., total inlet conditions normalized with respect to critical state properties, considered in this work is reported in Table 2.

Several techniques are suitable for data-driven regression, e.g., symbolic regression, Artificial Neural Networks (ANN), Support Vector Machines (SVM), Gaussian Processes (GP). In the present work, a Multi-Layer Perceptron (MLP), i.e., a feedforward ANN featuring one or multiple fully connected hidden layers, has been selected to accomplish this task. The reason is twofold. First, the computational overhead associated with the evaluation of the data-driven model is of primary importance for the target application. In general terms, the computational cost of a MLP model scales with the total number of neurons and is lower than the cost of evaluating, for instance, a model based on a GP or a SVM. At the same time, a MLP model requires a larger amount of training data to reach the same level of accuracy as a GP or a SVM. However, the availability of data is not a limiting factor in the present work, since the dataset is synthetically generated.

To reduce the number of input features used to train the ANN and to avoid the use of categorical input, i.e., a string identifying the name of the fluid, the data associated with the working fluid and the inlet thermodynamic conditions have been synthesized in two parameters. These are the fluid molecular complexity, measured as the number of active degrees of freedom of a molecule (Colonna and Guardone, 2006)

$$N = \frac{2M c_{v,id}(T_c)}{R}, \tag{16}$$

and the average value of the isentropic pressure–volume exponent (Kouremenos and Kakatsios, 1985) over the compression process

$$\overline{\gamma_{Pv}} = \frac{\log\left(\dfrac{P_{in}}{P_{out}}\right)}{\log\left(\dfrac{\rho_{in}}{\rho_{out}}\right)}. \tag{17}$$

A detailed analysis of the influence of these parameters on the design of centrifugal compressors can be found in Giuffre et al. (2022), and it is omitted here for brevity. The resulting vector of input features for the ANN reads

$$X = \left[\phi_{t1}, \ \psi_{is}, \ \alpha_2, \ \frac{R_3}{R_2}, \ k, \ N_{bl}, \ H_{r,pinch}, \ R_{r,pinch}, \right.$$
$$\left. \beta_{tt,target}, \ \dot{m}, \ N, \ \overline{\gamma_{Pv}}, \ \frac{\epsilon_b}{H_2}, \ \frac{\epsilon_t}{H_2}\right]. \tag{18}$$

The original dataset has been pre-processed by removing the compressor designs that are considered unfeasible or do not meet the required specifications. The criteria used to filter the dataset are:

- minimum acceptable efficiency at design point
  $\eta_{tt} \geq 0.5$;

Table 2

Design space selected to create the dataset used to train the data-driven compressor model.

Variable	Range	Fluid	N	T_r	P_r
β_{tt}	2.0–5.0	H_2	3.0	2.0	0.08
$\dot{m}$ [kg/s]	0.05–0.25	CO_2	7.0	0.9	0.2
ϕ_{t1}	0.05–0.2	Propane	19.08	0.65	0.015
ψ_{is}	0.6–1.2	R-134a	21.64	0.65 - 0.81	0.015 - 0.15
$\alpha_2[°]$	60–75	Isobutane	28.43	0.65	0.015
k	0.65–0.95	R-1233zd(E)	28.77	0.65 - 0.82	0.015 - 0.15
N_{bl}	10–20				
R_3/R_2	1.2–2.0				
$H_{r,pinch} = \dfrac{H_3 - H_2}{H_2(R_2/R_{pinch} - 1)}$	0.0–1.0				
$R_{r,pinch} = \dfrac{R_{pinch} - R_2}{R_3 - R_2}$	0.0–1.0				

Table 3

Design space and set of optimal hyperparameters.

Hyperparameter	Range	MLP_{obj}	MLP_{con}
L	4–6	5	6
$n^{[1]}$	5–200	199	60
$n^{[2]}$	5–200	199	94
$n^{[3]}$	5–200	200	44
$n^{[4]}$	5–200	144	63
$n^{[5]}$	5–200	42	68
$n^{[6]}$	5–200	–	70
α	10^{-4}–10^{-1}	$10^{-2.75}$	$10^{-2.89}$
mini-batch size	2^6–2^{10}	2^6	2^6

Table 4

Accuracy of the two MLP models evaluated on the test set.

Y	$mae = \dfrac{1}{n}\sum_{i=1}^{n}\| \hat{Y} - Y \|$	$mape = \dfrac{1}{n}\sum_{i=1}^{n}\dfrac{\| \hat{Y} - Y \|}{Y} \cdot 100$
β_{tt}	0.031 [–]	0.96%
η_{tt}	0.007 [–]	0.97%
OR	0.013 [–]	4.97%
$\dot{m}_{choke}$	0.004 [kg/s]	2.41%
Ω_{des}	1670 [rpm]	1.01%
$R_{1,h}$	10^{-5} [m]	0.31%
H_2	10^{-5} [m]	0.84%
$\beta_{2,bl}$	0.02 [°]	0.37%
R_4	$7 \cdot 10^{-4}$ [m]	1.06%

- minimum acceptable operating range at the design rotational speed $OR = \dfrac{\dot{m}_{max} - \dot{m}_{min}}{\dot{m}_{des}}\bigg|_{\Omega_{des}} \geq 0.05$;
- maximum allowable blade angle at impeller outlet to ensure stable compressor operation $\beta_{2,bl} \leq 0°$;
- maximum allowable deviation between the target and the computed values of pressure ratio $\Delta\beta_{tt} \leq 20\%$.

The filtered dataset is composed by 165k samples, thus reducing the computational cost associated to the training of the data-driven model by about 30%, without any loss of useful information. In order to enhance the accuracy of the MLP model, input features standardization has been applied prior to training. Moreover, to further simplify the multivariate regression function to be learnt by the ANN, the labels have been categorized according to their use in the ECS optimization process, i.e., objectives or constraints. Then, two separate MLP models have been trained to predict the vector of objective functions and constraints, namely:

$$Y_{obj} = [\beta_{tt}, \eta_{tt}, OR, \dot{m}_{choke}],$$
$$Y_{con} = [\Omega_{des}, R_{1,h}, H_2, \beta_{2,bl}, R_4]. \tag{19}$$

Upon pre-processing, the dataset has been split into training, development, and test sets, counting 145k, 10k, and 10k samples, corresponding to approximately 88%, 6%, and 6% of the total amount of data, respectively. The space of hyperparameters investigated to optimize the accuracy of the ANN is summarized in Table 3. The hyperparameters search is performed by resorting to the NOMAD algorithm (Audet et al., 2019, 2021), i.e., an optimization algorithm suited for mixed-integer non-linear programming problems, featuring an expensive black-box function evaluation. For each combination of hyperparameters, a MLP model is created leveraging an open-source programming framework (Abadi et al., 2015). The model is trained for 80 epochs, and its performance is evaluated on the development set, using the mean squared error loss function

$$L(\theta) = \frac{1}{n}\sum_{i=1}^{n}(\hat{y}_i - y_i)^2, \tag{20}$$

where θ, n, and $\hat{y}$ denote the space of the hyperparameters, the number of samples, and the model prediction, respectively. The optimal

architecture is selected after a maximum of 750 different MLP models have been trained and evaluated. The process is repeated for both the models trained to predict Y_{obj} and Y_{con}. The hyperparameters search has been performed on an Intel® Xeon® Gold 5220R, featuring 48 logical threads, leading to a total computational cost of about 380 h. The arrays of optimal hyperparameters are reported in Table 3 for the two MLP models. The training histories of the MLP models featuring the optimal set of hyperparameters are displayed in Fig. 6.

The accuracy of the optimal MLP models is evaluated for each label on the test set, i.e., the 10k samples not used for training or hyperparameters search, in terms of both mean absolute error (mae), and mean absolute percentage error (mape). The results are listed in Table 4. Furthermore, to provide a more comprehensive overview of the predictive capabilities of the MLPs, the deviation between the model predictions and the true labels of the test set is reported in Fig. 7. The comparison shows an excellent agreement, and highlights that the maximum prediction errors occur when the value of the operating range is close to zero.
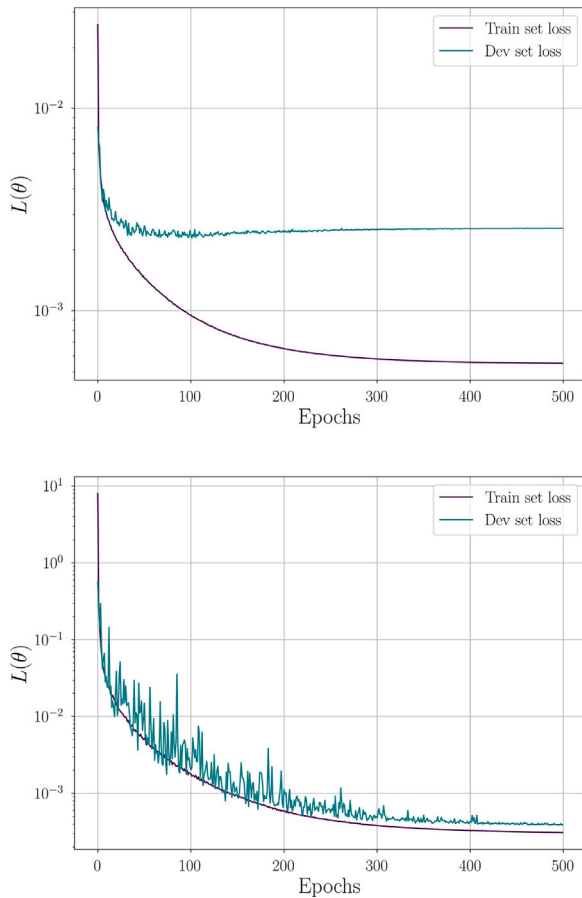
3.4. ECS design optimization

The optimization of an aircraft ECS is a multi-disciplinary problem involving aspects related, but not limited, to: system performance, weight, installation, maintenance, safety, and life-cycle costs. For the sake of simplicity, the present study addresses an optimization problem involving three conflicting objectives, namely the maximization of the system COP, and the minimization of the weight and of the drag penalty associated to the ram airflow. With the purpose of evaluating the overall performance of the ECS, the COP is defined as the ratio of the power required for cabin cooling and pressurization in ideal conditions, over the total electric power consumption of the system, due to the cabin air compressor, the ram air fan and the high-speed centrifugal compressor:

$$COP = \frac{\dot{Q}_{cooling} + \dot{W}_{p,id}}{\dot{W}_{el,CAC} + \dot{W}_{el,fan} + \dot{W}_{el,CC}}. \tag{21}$$

To further simplify the problem, only the dry weight of the two CHEXs is accounted for as objective in the optimization process. The

Table 5
Settings of the multi-objective optimization problem.

Design variable	Type	Range	Constraint	Value
$\dot{m}_{\mathrm{ram}}$ [kg/s]	System	0.4–1.0	$\min(R_{1,\mathrm{h}})$ [mm]	3.25
$\dot{m}_{\mathrm{refr}}$ [kg/s]	System	0.1–0.25	$\min(H_2)$ [mm]	1.5
β_{tt}	System	2.0–5.0	$\min(\beta_{2,\mathrm{bl}})$ [°]	−45
ΔT_{sh} [K]	System	3.0–10.0	$\max(\beta_{2,\mathrm{bl}})$ [°]	−10
ΔT_{sc} [K]	System	3.0–10.0	$\max(\Omega)$ [krpm]	250
ϕ_{t1}	Compressor	0.05–0.2	$\min(x)\big|_{\mathrm{eva-cond}}$ [mm]	50
ψ_{is}	Compressor	0.6–1.0	$\max(x)\big|_{\mathrm{eva-cond}}$ [mm]	800
α_2 [°]	Compressor	60–75	$\min(\Delta T_{\mathrm{pp}})\big|_{\mathrm{eva}}$ [K]	3
k	Compressor	0.65–0.95	$\min(\Delta T_{\mathrm{pp}})\big|_{\mathrm{cond}}$ [K]	5
N_{bl}	Compressor	10–20	$\max(V_{\mathrm{air}})\big|_{\mathrm{eva-cond}}$ [m/s]	30
R_3/R_2	Compressor	1.2–2.0	$\max(V_{\mathrm{refr}})\big|_{\mathrm{eva-cond}}$ [m/s]	30
$R_{\mathrm{r,pinch}}$	Compressor	0.0–1.0		
$H_{\mathrm{r,pinch}}$	Compressor	0.0–1.0		
$y\big|_{\mathrm{eva-cond}}$ [mm]	Heat exchanger	100–300		
$z\big|_{\mathrm{eva}}$ [mm]	Heat exchanger	20–70		
$z\big|_{\mathrm{cond}}$ [mm]	Heat exchanger	10–60		

Fig. 6. Training history of MLP models trained to predict Y_{obj} (top) and Y_{con} (bottom), and featuring the optimal set of hyperparameters.

can be formulated as follows:

$$\min_{\boldsymbol{\alpha}\in\mathbb{R}^n} F(\boldsymbol{\alpha}) = [f_1(\boldsymbol{\alpha}), \dots, f_{n_{\mathrm{obj}}}(\boldsymbol{\alpha})], \quad \text{s.t.}$$
$$h_k(\boldsymbol{\alpha}) = 0 \quad k = 1, \dots, n_{\mathrm{eq}}$$
$$g_i(\boldsymbol{\alpha}) \leq 0 \quad i = 1, \dots, n_{\mathrm{ineq}} \tag{22}$$
$$\alpha_{l,j} \leq \alpha_j \leq \alpha_{u,j} \quad j = 1, \dots, n$$

where $\boldsymbol{\alpha}$ is the vector of design variables, $F(\boldsymbol{\alpha})$ is the vector of the objective functions, and $h_k(\boldsymbol{\alpha})$, $g_i(\boldsymbol{\alpha})$ are the vectors of the equality and inequality constraints, respectively. The non-linear constraints are imposed to ensure the manufacturability of the system components, i.e., heat exchangers and compressor, and to define an upper threshold for the speed of the air and the refrigerant in the circuit. Overall, the optimization problem comprises 17 design variables, 3 objectives, and 15 inequality constraints, as summarized in Table 5. In line with what is reported in the introduction, this demonstrates that the size of the optimization problem rapidly increases, when including the design of the centrifugal compressor in the integrated design framework together with a set of realistic manufacturing constraints.

The in-house optimization framework consists of a Python program coupling the ECS model developed in Modelica with an open-source toolbox for multi-objective design optimization (Blank and Deb, 2020). The Pareto front of optimal solutions is computed by means of the NSGA-II algorithm described in Deb et al. (2002). The initial population comprises ten individuals for each design variable, and is sampled according to the latin hypercube methodology along the floating-point directions, and randomly along the integer axis, i.e., the one corresponding to the number of compressor blades. The population is evolved for a maximum of 170 generations, leading to a maximum of 28900 evaluations of the Modelica model. The result thereof is that the computational cost quickly becomes prohibitive when increasing the number of design variables, even if resorting to parallel computing to evaluate the individuals of each generation.

To overcome this limitation, the integrated design framework has been modified by replacing the compressor model implemented in Modelica with the pre-trained MLP models described in the previous section. The computational cost of the optimization problem can be significantly reduced by limiting the number of design variables selected by the stochastic algorithm NSGA-II. This can be achieved by leveraging the computational efficiency of the pre-trained MLP models, as described in the following. The vector of design variables $\boldsymbol{\alpha}$ can be conveniently split into three subsets, corresponding to the design variables of the system, the heat exchangers, and the high-speed compressor:

$$\boldsymbol{\alpha}_{\mathrm{sys}} = [\dot{m}_{\mathrm{ram}}, \dot{m}_{\mathrm{refr}}, \beta_{\mathrm{tt}}, \Delta T_{\mathrm{sh}}, \Delta T_{\mathrm{sc}}],$$
$$\boldsymbol{\alpha}_{\mathrm{HEX}} = [y\big|_{\mathrm{eva}}, y\big|_{\mathrm{cond}}, z\big|_{\mathrm{eva}}, z\big|_{\mathrm{cond}}], \tag{23}$$
$$\boldsymbol{\alpha}_{\mathrm{c}} = [\phi_{\mathrm{t1}}, \psi_{\mathrm{is}}, \alpha_2, k, N_{\mathrm{bl}}, R_3/R_2, R_{\mathrm{r,pinch}}, H_{\mathrm{r,pinch}}].$$

weight of the remaining components of the ECS is assumed to be constant throughout the design space. Due to the low operating temperature of the prescribed application, the material selected for both the condenser and the evaporator is the Aluminium alloy 6061. The weight minimization leads to CHEXs designs characterized by a high heat transfer surface-to-volume ratio. This design approach is beneficial in terms of heat transfer efficiency, but it often leads to higher pressure drops. To compensate for this effect, the third objective function selected in the present study addresses the minimization of the ram air drag. In mathematical form, the multi-objective optimization problem
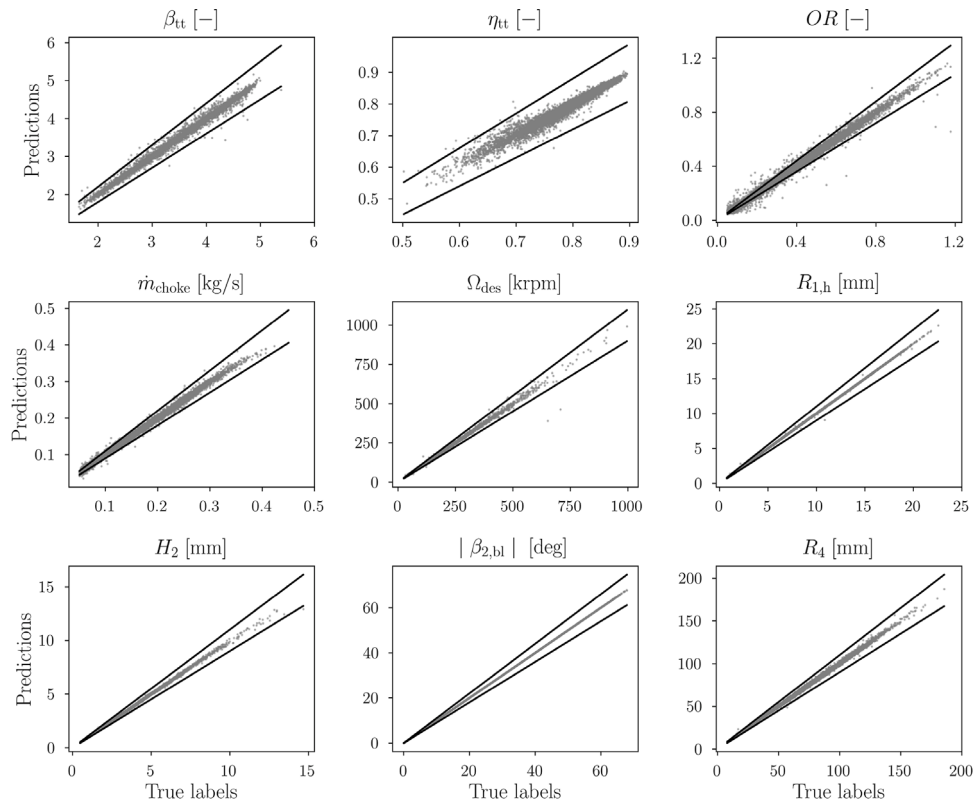
Fig. 7. Comparison between the predictions of the optimal MLP models and the true labels of the test set. The data points are displayed in gray, whereas the black lines correspond to the $\pm 10\%$ error bands.
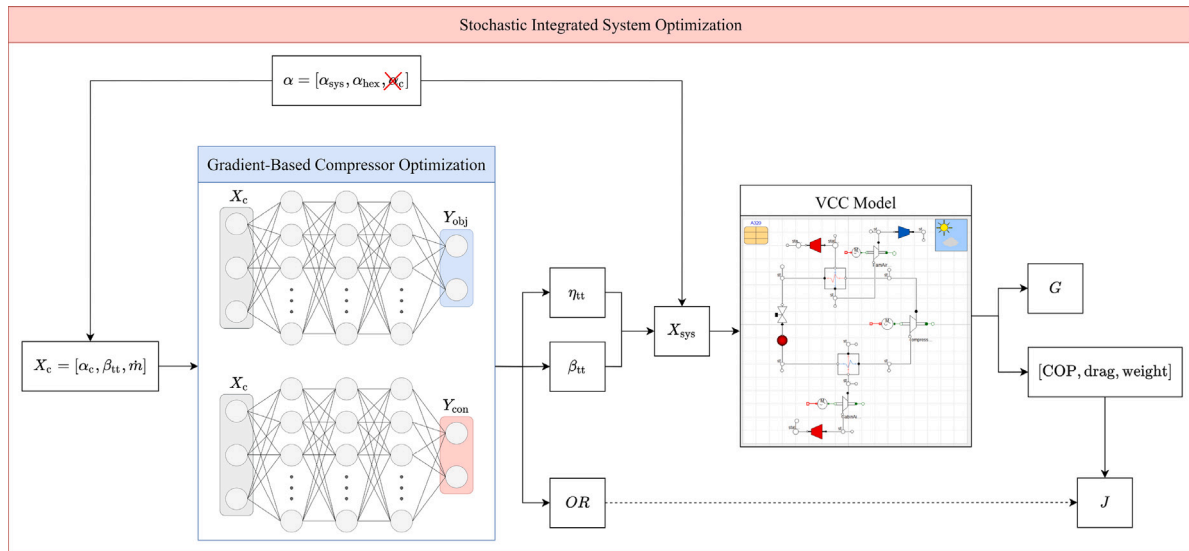

Fig. 8. Flowchart of the modified ECS optimization framework. The data-driven model is used to decouple the optimization of the high-speed centrifugal compressor, highlighted in blue, from the optimization of the VCC system, highlighted in red. (For interpretation of the references to color in this figure legend, the reader is referred to the web version of this article.)

The vector of input features for the data-driven model can be assembled by combining α_c with two variables of α_{sys}, namely, $\dot{m}_{refr}$, β_{tt}, and with two parameters related to compressor manufacturability, i.e., ϵ_b/H_2, ϵ_t/H_2, and two parameters related to the prescribed working fluid and thermodynamic state, i.e., N, $\overline{\gamma_{Pv}}$. As a result, the set of compressor design variables α_c can be decoupled from the array of optimization variables selected by the stochastic algorithm, and can be

treated separately. In the present implementation, once the values of β_{tt} and $\dot{m}_{refr}$ have been selected by the stochastic algorithm for each individual of a generation, the set of α_c is optimized separately, by resorting to a constrained gradient-based algorithm (Kraft, 1988). The values of the objectives and constraints are evaluated by means of the MLP models, and the objective function is expressed as a linear combination of η_{tt} and OR. After the gradient-based optimization, the resulting

values of η_{tt} and β_{tt} are appended to the vectors $\boldsymbol{\alpha}_{sys}$ and $\boldsymbol{\alpha}_{HEX}$, and the values of the objectives and the constraints of the VCC system are evaluated by means of the Modelica model. Eventually, the compressor operating range can be included into the vector of objective functions $\boldsymbol{J}$. However, this is not done in the present work, since the aim is to compare the Pareto front identified by means of the original and the modified ECS optimization framework, without altering the vector of the objective functions. The proposed optimization methodology is schematically illustrated in Fig. 8.

Thanks to the use of data-driven modeling, the cost of the compressor optimization for each individual of the population is negligible, as compared to the cost associated with the evaluation of the VCC system model. On the other hand, the number of design variables selected by the stochastic algorithm drops from 17 to 9, leading to a sizeable reduction of the number of objective function evaluations required to reach convergence.

4. Results

The test case selected to benchmark the performance of the original and the modified integrated design framework is the multi-objective optimization of an electrically-driven VCC system for the ECS of a single-aisle, short-haul aircraft, e.g., the Airbus A320. The aircraft is assumed to fly at cruise conditions, namely at $M_\infty = 0.78$, and at an altitude of $11.88\,\mathrm{km}$. The environmental conditions are computed according to the International Standard Atmosphere (ISA) model. The working fluid selected for the VCC system is refrigerant R-134a. The inlet conditions of the mixing manifold of the air distribution system, which corresponds to the outlet of the VCC system, are specified in terms of mass flow rate, pressure, and temperature: $\dot{m}_{mix} = 0.5\,\mathrm{kg/s}$, $P_{mix} = 76.25\,\mathrm{kPa}$, $T_{mix} = 13.14\,°\mathrm{C}$, and correspond to a mild cooling operating point (Sielemann et al., 2011). The water content in the air at cruise altitude is negligible, thus the effect of humidity is disregarded. The objectives selected for the optimization study are the system COP, the weight of the CHEXs, and the drag penalty associated with the ram airflow. The design variables and the non-linear constraints are listed in Table 5. The results are computed and presented for a single ECS pack.

The multi-objective optimization performed with the original framework, namely the one adopting the compressor model embedded in Modelica, reached convergence after a total of 13050 function evaluations. Conversely, the number of function evaluations reduces to 4500 when resorting to the modified optimization framework, leveraging the data-driven compressor model. This enables a reduction of the total computational time from approximately 125 h to 37.5 h when running the optimization in parallel on an Intel® Xeon® E5-1620 v3 CPU, featuring 8 logical threads. The Pareto front computed with the modified optimization framework is displayed in Fig. 9. The COP of the entire ECS, see Eq. (21), is reported on the x-axis of the left figure, whereas the COP of the VCC system, i.e., the ratio between the cabin cooling duty ($\dot{Q}_{cooling}$) and the electrical power required by the centrifugal compressor ($\dot{W}_{el,CC}$), is reported on the x-axis of the right chart. The same results are illustrated on the weight-drag, COP-weight, and COP-drag planes in Fig. 10. By comparing the optimal design points identified with the original and the modified integrated design methodology, it is possible to observe that: (i) similar trends are established among the three objectives; (ii) the range of variation of weight and drag penalty over the Pareto front is comparable; (iii) the design methodology exploiting the data-driven compressor model is able to identify optimal solutions characterized by higher COP.

Additional insights regarding the optimal VCC system configurations identified with the framework embedding the data-driven compressor model can be inferred by examining the data reported in Table 6. In particular, the table lists the design variables and the main performance metrics corresponding to the design points leading to maximum COP, minimum drag penalty, and minimum weight.

Moreover, a VCC system layout corresponding to an optimal trade-off solution, i.e., the one leading to the minimum fuel weight penalty W_{f0}, is reported in Table 6. In this work, the fuel weight penalty associated with the ECS is computed as the sum of three contributions (SAE, 2004):

- penalty due to additional weight

$$W_{f0} = W_{ECS} \left[\exp\left(\frac{SFC_{th}\tau}{L/D} \right) - 1 \right];$$ (24)

- penalty associated with shaft power off-take

$$W_{f0} = P_{el} SFC_P \frac{L/D}{SFC_{th}} \left[\exp\left(\frac{SFC_{th}\tau}{L/D} \right) - 1 \right];$$ (25)

- penalty associated with ram air drag

$$W_{f0} = \dot{m}_{ram} v_{air} \frac{L/D}{g} \left[\exp\left(\frac{SFC_{th}\tau}{L/D} \right) - 1 \right].$$ (26)

The values of the parameters in Eq. (24)–(26) depend on the aircraft type, the engine specifications, and the prescribed flight phase. The set of aircraft parameters selected in this work are representative of an Airbus A320 flying at cruise and is reported in Table 7.

Analyzing the optimal VCC system configurations reported in Table 6, the following design considerations can be derived. As the cabin cooling requirement is fixed in the present study, the COP of the system is inversely proportional to the power demand of the refrigerant compressor. It follows that, to maximize the COP, the pressure ratio provided by the compressor has to be minimized, as displayed in Fig. 11. This design choice implies that the condenser operates at a lower pressure level and its core dimensions become larger, with a consequent reduction of the pressure losses on the refrigerant side. With reference to Fig. 4, this can be achieved by increasing z_{eva} and z_{cond}, thus lowering the refrigerant velocity in the microchannels. The analysis of Fig. 11 reveals also the main reason of the difference in the COP computed with the original and the modified optimization framework. The use of the data-driven compressor model leads to optimal solutions featuring a wider range of β_{tt}, thus a wider range of COP values. The root cause of this difference can be arguably attributed to the higher complexity of the VCC system model when embedding the compressor meanline code. This makes the solution of the underlying non-linear system of equations more susceptible to failure during the optimization process, narrowing the design space that the optimizer can explore.

On the other hand, if the main objective is to design compact and lightweight heat exchangers, it is necessary to minimize the heat transfer surfaces, i.e., minimize the x, y, and z dimensions of the condenser and the evaporator. This can be accomplished by raising the pressure ratio provided by the refrigerant compressor, which results in an increase of the temperature lift, i.e., the difference between T_{cond} and T_{eva}. This design choice does not lead only to higher electric power consumption, but also to larger drag penalty due to larger pressure drops in the air flow. The increase of P_{el} is exacerbated by the increment of the refrigerant mass flow rate observed in the case of more compact heat exchanger designs, as depicted in Fig. 12. This trend can be explained by observing that, given a value of evaporation pressure, the latent heat of condensation decreases with an increase in the pressure ratio and temperature lift. In turn, since the condenser heat duty does not vary significantly throughout the Pareto front, a higher refrigerant mass flow rate is required when higher values of pressure ratio are chosen.

Conversely, in order to minimize the drag penalty, the designer has to select an intermediate value of pressure ratio and minimize the pressure drops on the ram air side. This can be achieved by increasing the condenser frontal area on the air side, i.e., $A_{cond,air} = x_{cond} \cdot y_{cond}$, which results in lower air velocity throughout the condenser, at a given mass flow rate. This argument is corroborated by the trend displayed in Fig. 13.
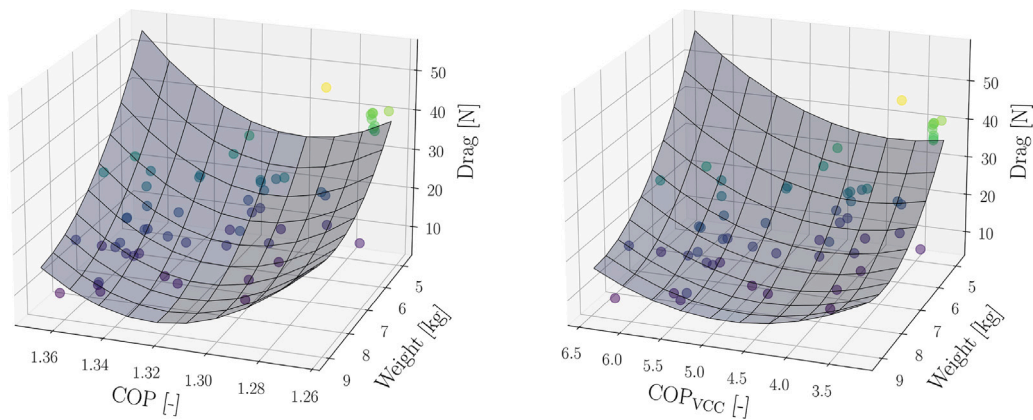
Fig. 9. Pareto front computed with the modified optimization framework coupled to the data-driven compressor model, considering the COP of the entire ECS (left), and the COP of the VCC system (right).
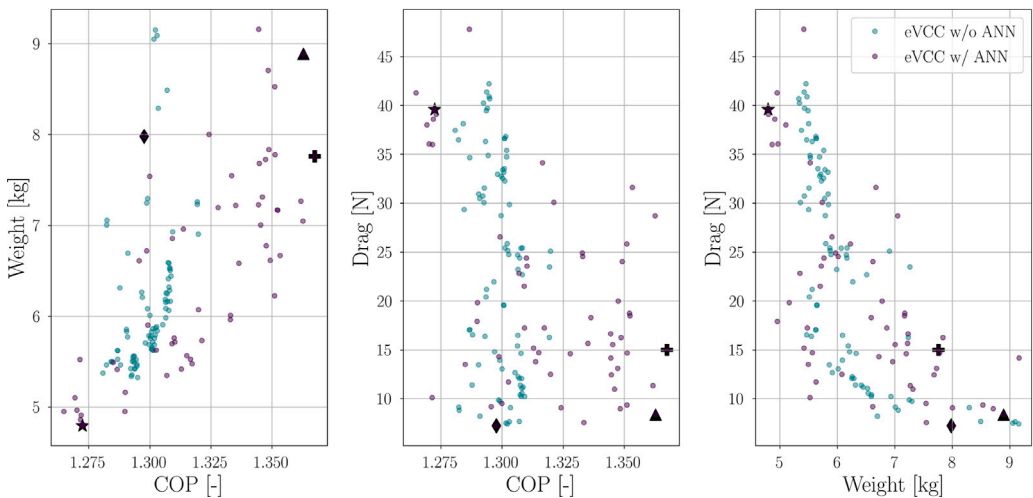

Fig. 10. Comparison between the trends established among the objective functions, computed with and without the use of the data-driven compressor model, coupled to the integrated design optimization framework. The markers identify the optimal solutions reported in Table 6.
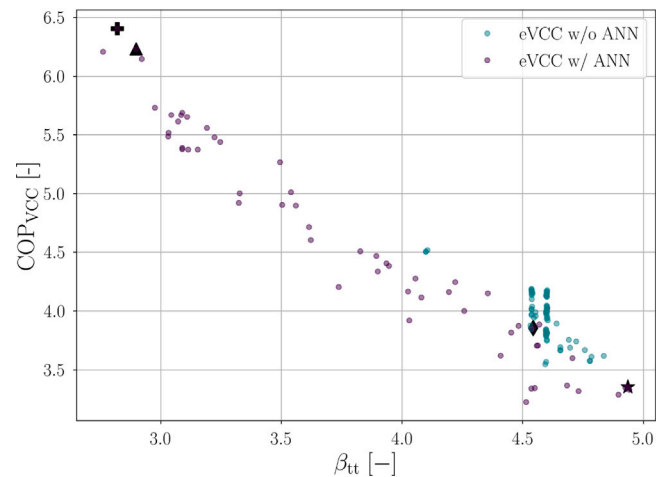

Fig. 11. COP of the VCC system vs. total-to-total pressure ratio, computed for the ECS models with and without the data-driven model of the centrifugal compressor. The markers identify the optimal solutions reported in Table 6.

Fig. 12. CHEXs weight vs. refrigerant mass flow rate, computed for the ECS models with and without the data-driven model of the centrifugal compressor. The markers identify the optimal solutions reported in Table 6.
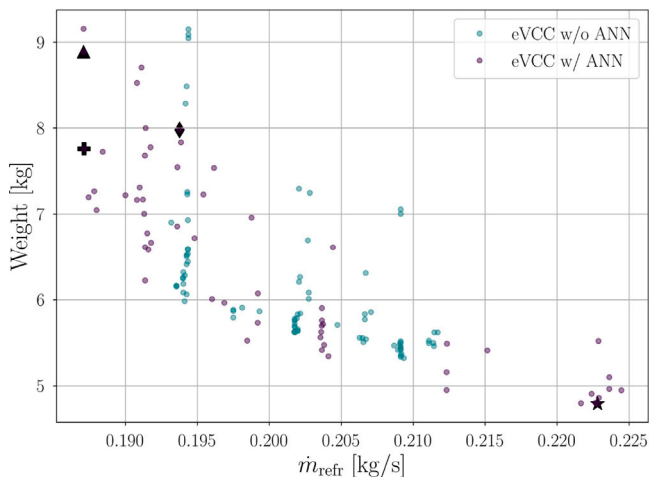
Table 6

Most influential design variables and performance metrics corresponding to the optimal VCC system configurations selected over the Pareto front computed with the data-driven model. The optimal design points leading to maximum COP, minimum drag, minimum weight, and minimum fuel weight penalty are marked with different symbols.

| Symbol	Type	✚ max(COP)	◆ min(drag)	★ min(weight)	▲ min(W_{f0})
$\dot{m}_{\text{ram}}$ [kg/s]	System - variable	0.99	0.97	0.99	0.86
$\dot{m}_{\text{refr}}$ [kg/s]	System - variable	0.19	0.19	0.22	0.19
β_{tt} [–]	System - variable	2.8	4.5	4.9	2.9
COP [–]	System - result	1.4	1.3	1.3	1.4
COP_{VCC} [–]	System - result	6.4	3.8	3.4	6.2
Weight [kg]	System - result	7.8	8.0	4.8	8.9
Drag [N]	System - result	15.0	7.2	39.6	8.4
W_{f0} [kg]	System - result	32.2	33.2	36.0	31.6
P_{el} [kW]	System - result	65.3	68.8	69.7	65.0
$\dot{Q}_{\text{eva}}$ [kW]	System - result	32.3	32.3	32.0	32.0
$\dot{Q}_{\text{cond}}$ [kW]	System - result	37.1	40.2	41.1	36.8
P_{eva} [bar]	System - result	2.07	1.34	2.23	2.17
P_{cond} [bar]	System - result	5.72	6.15	10.70	6.14
T_{eva} [K]	System - result	263.9	253.4	265.8	265.2
T_{cond} [K]	System - result	293.1	295.5	315.1	295.5
z_{eva} [mm]	Heat exchanger - variable	70	60	60	61
z_{cond} [mm]	Heat exchanger - variable	51	41	51	51
$A_{\text{eva,air}}$ [m^2]	Heat exchanger - result	0.10	0.08	0.11	0.12
$A_{\text{cond,air}}$ [m^2]	Heat exchanger - result	0.21	0.33	0.09	0.26
$\Delta P_{\text{air,eva}}$ [kPa]	Heat exchanger - result	2.13	2.05	1.38	1.29
$\Delta P_{\text{air,cond}}$ [kPa]	Heat exchanger - result	2.71	1.07	8.28	1.82
$\Delta P_{\text{refr,eva}}$ [kPa]	Heat exchanger - result	3.67	4.59	4.64	3.72
$\Delta P_{\text{refr,cond}}$ [kPa]	Heat exchanger - result	0.59	1.37	1.06	0.59
ϕ_{t1} [–]	Compressor - variable	0.07	0.10	0.06	0.05
ψ_{is} [–]	Compressor - variable	0.81	0.80	0.79	0.83
α_2 [°]	Compressor - variable	70.1	69.5	70	67.3
η_{tt} [–]	Compressor - result	0.85	0.81	0.84	0.85
Ω [krpm]	Compressor - result	52	100	55	39
$R_{1,\text{h}}$ [mm]	Compressor - result	5.3	6.8	5.5	5.3
H_2 [mm]	Compressor - result	3.0	3.0	2.9	2.8
$\beta_{2,\text{bl}}$ [°]	Compressor - result	−33.5	−33.1	−35.6	−25.7

Table 7

Set of aircraft parameters prescribed for the calculation of the fuel weight penalty. The values are representative of an Airbus A320 flying at cruise (Bender, 2018).

Parameter	Value
SFC_{th} [lb/(lbf.h)]	0.514
SFC_{p} [lb/(hp.h)]	0.5
L/D [–]	15.32
τ [h]	1.5

The trade-off solution leading to the minimum fuel weight penalty can be interpreted as a linear combination of the VCC system configurations associated with maximum COP and minimum drag penalty. In particular, the pressure ratio and the refrigerant mass flow rate delivered by the compressor resemble the values leading to maximum COP. In the same fashion, the frontal area of the condenser on the ram air side is close to the value associated with minimum drag penalty. Moreover, the values of the pressure drops on the refrigerant side are comparable to those leading to maximum COP, whereas the values of the pressure drops on the air side are similar to those computed for the system layout featuring minimum drag. Nevertheless, it should be noted that in real applications the ECS must be sized not only to operate at cruise conditions but also at critical operating points, such as ground operation on a very hot and humid day. To comply with such extreme cooling requirements, the heat exchangers are oversized with respect to what is reported in this work. Moreover, additional weight contributions, e.g., the weight of the turbomachines, can be included in Eq. (24). As a result, the weight of the ECS of an actual passenger aircraft may have a higher influence on the fuel weight penalty than estimated in the present work.

A detailed analysis of the trends established among the most influential performance metrics of the refrigerant compressor is presented in Fig. 14. The values of η_{tt} depicted in the figure correspond to the
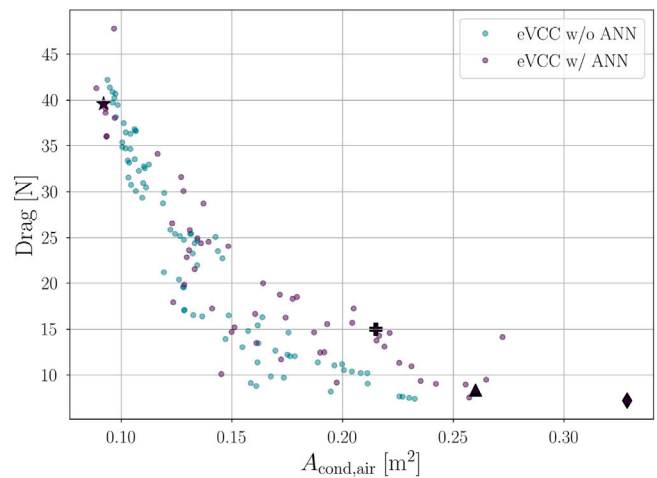
Fig. 13. Drag penalty vs. condenser frontal area on the air side, computed for the ECS models with and without the data-driven model of the centrifugal compressor. The markers identify the optimal solutions reported in Table 6.

internal efficiency, which only accounts for the losses occurring within the main flow passage. The external losses, e.g., the windage loss, are taken into account when calculating the power demand of the compressor. As expected, the compressor efficiency is inversely proportional to the pressure ratio. Moreover, the design points associated with ECS configurations with maximum COP and minimum fuel weight penalty lie in the region of maximum compressor efficiency. In general terms, an increase in the pressure ratio leads to compressor designs featuring higher values of the rotational speed. This can be mainly attributed to the need for a higher value of peripheral speed to achieve a higher specific work. The ECS configuration featuring the compressor with the highest rotational speed is the one leading to minimum drag. This can be explained by the fact that the compressor weight is not
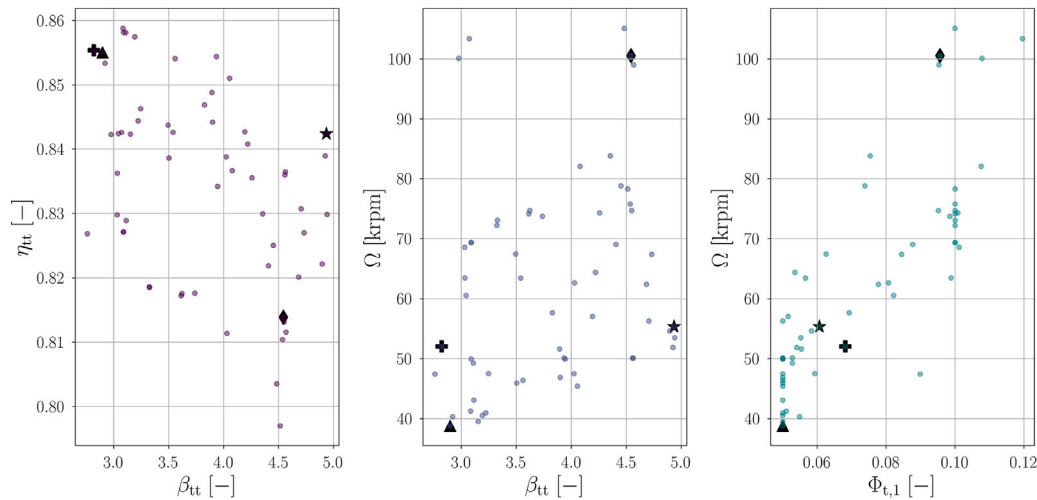
Fig. 14. Trends of compressor efficiency and rotational speed as a function of pressure ratio, and trend of rotational speed as a function of swallowing capacity established over the Pareto front computed with the data-driven model. The markers identify the optimal solutions reported in Table 6.

taken into account in the objective function and by the fact that the evaporating pressure P_{eva} is lower at the compressor inlet. In turn, this leads to a higher volumetric flow rate processed by the compressor, and, consequently, to a higher swallowing capacity selected by the optimizer. As documented in Giuffre et al. (2022), higher values of $\Phi_{t,1}$ are associated with higher rotational speeds, but also with lower values of operating range, thus limiting the operating envelope that can be covered by the VCC system. To overcome this issue, in the modified integrated design framework, the compressor optimization has been performed by setting a linear combination of η_{tt} and OR as one of the objective functions. This explains the presence of optimal design points, e.g., the one associated with minimum fuel weight penalty, characterized by values of the compressor swallowing capacity in the order of 0.05.

To conclude the study, a sensitivity analysis of the objective functions with respect to the prescribed set of design variables is performed. The purpose is to assess the robustness of the solutions with respect to changes in the values of the design variables, as well as to identify those variables which mostly affect the objective functions. The analysis is carried out as follows. First, five design points are selected over the Pareto front computed with the modified optimization framework. Then, a perturbation of $\pm 10\%$ is applied to each design variable independently, and the vector of objective functions is re-evaluated. This process is repeated for each prescribed design point, and the averaged results are displayed in Fig. 15. The sensitivity of the objective functions is evaluated with respect to the compressor efficiency η_{tt}, rather than to the compressor design variables α_c. Moreover, for the present investigation, the COP of the ECS is replaced with the COP of the VCC system, since the former is mainly affected by the terms $\dot{W}_{p,id}$ and $\dot{W}_{el,CAC}$ in Eq. (21), whose values are almost constant in the simulations.

The outcomes of the sensitivity analysis can be summarized as follows. The COP shows the highest sensitivity with respect to the mass flow rate of the refrigerant, and to the pressure ratio and the efficiency of the refrigerant compressor. The weight of the CHEXs is mostly affected by the mass flow rates of refrigerant and ram air. The value of drag penalty shows the highest sensitivity with respect to $\dot{m}_{refr}$, $\dot{m}_{ram}$, z_{cond}, y_{eva}, and β_{tt}. As a result, the computational cost of the optimization process can be further reduced by removing z_{eva}, y_{cond}, ΔT_{sh}, and ΔT_{sc} from the vector of design variables, without significantly affecting the optimal solutions. Moreover, the COP of the optimal designs shows a variation of the order of $\pm 10\%$ when changing the values of the compressor efficiency and the refrigerant mass flow rate by the same order of magnitude. These results corroborate the fact

that the compressor is one of the most critical components of the VCC system, and highlight the need of performing its conceptual design along with that of the system.

5. Conclusions

A novel integrated design optimization method for aircraft ECS, based on the electrically-driven VCC system, has been presented in this work. The main novelty lies in the integration of the conceptual design of the high-speed compressor, performed by means of a data-driven model, as well as of the compact heat exchangers, along with the definition of the VCC system cycle parameters. The case study selected to demonstrate the capabilities of the proposed methodology is the multi-objective design optimization of an electrically-driven VCC system for the ECS of a single-aisle, short-haul aircraft, flying at cruise conditions. The prescribed objective functions are the maximization of the system COP, the minimization of the weight of the heat exchangers, and the minimization of the drag penalty associated with the ram airflow. The optimization of the VCC system has been performed with and without the use of the data-driven compressor model, to highlight the advantages offered by the proposed methodology. The main outcomes can be summarized as follows.

1. A data-driven compressor model can be developed using a dataset of about 165k compressor designs. The number of design variables considered to create the dataset is relatively limited, thanks to the adoption of a non-dimensional approach based on scaling principles. To enhance the accuracy of the data-driven model, and to facilitate its integration in the ECS optimization framework, two MLP models have been trained to predict the compressor performance parameters and the relevant geometrical constraints. The mean absolute percentage error of the two MLP models evaluated on the test set is 2.32% and 0.72%, respectively.
2. The complexity of the VCC system model, and the likelihood of an ill-conditioned matrix when the associated mathematical problem is solved, can be reduced by replacing the high-speed centrifugal compressor with a data-driven model. A similar approach could be adopted to replace also the models of the compact heat exchangers.
3. The use of a data-driven model enables the partial decoupling between the optimization of the VCC system and of the compressor. For each set of system design variables selected by the stochastic algorithm, the compressor design variables are optimized by resorting to a constrained gradient-based algorithm.
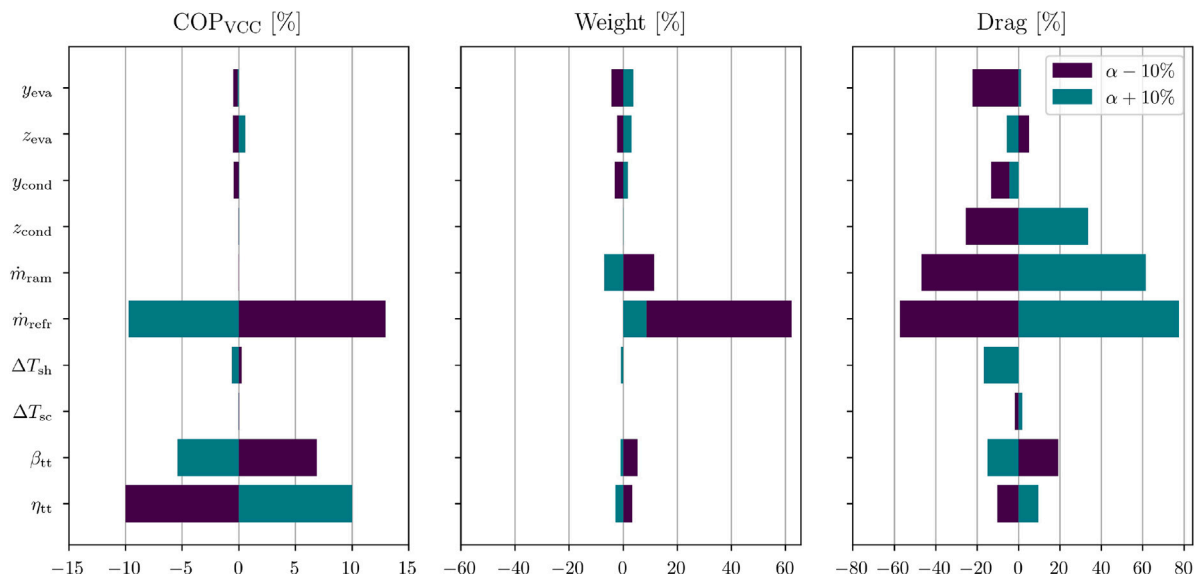
Fig. 15. Sensitivity of the objective functions with respect to a ±10% perturbation in the vector of design variables. The analysis is repeated for five optimal design points selected over the Pareto front identified with the modified optimization framework, and the results are averaged.

As a result, the number of design variables selected by the stochastic algorithm drops from 17 to 9, and the number of function evaluations needed to identify the Pareto front reduces from 13050 to 4500.

4. The objective functions selected for the optimization of the VCC system are in trade-off. In particular, the use of very compact heat exchangers leads to higher drag penalties. Nevertheless, it is possible to achieve a lightweight design of the heat exchangers, without incurring in large drag penalties, at the expense of a reduction in the COP. The range of variation of the objective functions and the trends established among them remain virtually unaltered, regardless of the adopted compressor model. Moreover, the modified framework is able to identify optimal solutions in a wider design space, thanks to the improved robustness of the underlying VCC system model.

5. The results show that the ram airflow and the condenser thermal load do not vary significantly over the Pareto front. Therefore, the use of heavier condenser units, featuring a larger frontal area on the ram air side, leads to a reduction of the drag penalty. On the other hand, the adoption of compact and lightweight heat exchangers requires a higher temperature lift and a higher refrigerant mass flow rate to comply with the prescribed heat duty.

6. An increase in the temperature lift of the VCC system produces a rise in the pressure ratio of the refrigerant compressor. In turn, this leads to a rapid deterioration of the compressor efficiency and to an increase in the rotational speed. A higher rotational speed, thus a more compact compressor design, can be also attained by increasing the value of the swallowing capacity. However, this comes at the expense of a reduced operating range.

7. As pointed out by a sensitivity analysis, the computational cost of the optimization process can be further reduced by removing z_{eva}, y_{cond}, ΔT_{sh}, and ΔT_{sc} from the vector of design variables, without significantly affecting the solution. Furthermore, the analysis shows that the COP of the VCC system is mostly influenced by the compressor efficiency. This demonstrates the need for an integrated design optimization methodology embedding a model for the conceptual design of the compressor.

The results of this research reveal the large potential of adopting data-driven models for the simultaneous optimization of a refrigeration cycle and the preliminary design of its components. The substantial reduction of the computational cost associated with the optimization process, combined with the improved robustness of the underlying system model, make this approach suitable for large-scale, industrial-strength design applications. Future works will target the improvement of the data-driven compressor model by extending the dataset with additional working fluids and thermodynamic conditions. Furthermore, the proposed integrated design methodology will be applied to assess the performance of different non-conventional ECS architectures over multiple operating points.

CRediT authorship contribution statement

Andrea Giuffre': Conceptualization, Methodology, Data-driven model, ECS system model, Software, Validation, Data curation, Writing – original draft. **Federica Ascione:** Conceptualization, Methodology, ECS system model, Software, Validation, Data curation, Writing – original draft. **Carlo De Servi:** Conceptualization, Supervision, Writing – review & editing. **Matteo Pini:** Conceptualization, Supervision, Writing – review & editing.

Declaration of competing interest

The authors declare that they have no known competing financial interests or personal relationships that could have appeared to influence the work reported in this paper.

Acknowledgments

References

Abadi, M., Agarwal, A., Barham, P., Brevdo, E., Chen, Z., Citro, C., Corrado, G.S., Davis, A., Dean, J., Devin, M., Ghemawat, S., Goodfellow, I., Harp, A., Irving, G., Isard, M., Jia, Y., Jozefowicz, R., Kaiser, L., Kudlur, M., Levenberg, J., Mané, D., Monga, R., Moore, S., Murray, D., Olah, C., Schuster, M., Shlens, J., Steiner, B., Sutskever, I., Talwar, K., Tucker, P., Vanhoucke, V., Vasudevan, V., Viégas, F., Vinyals, O., Warden, P., Wattenberg, M., Wicke, M., Yu, Y., Zheng, X., 2015. TensorFlow: Large-scale machine learning on heterogeneous systems. URL https://www.tensorflow.org/.

ACARE, 2017. Strategic research and innovation agenda. Technical report, Advisory Council for Aviation Research and Innovation in Europe.

Amirante, R., De Bellis, F., Distaso, E., Tamburrano, P., 2015. An explicit, non-iterative, single equation formulation for an accurate one dimensional estimation of vaneless radial diffusers in turbomachines. J. Mech. 31 (2), 113–122. http://dx.doi.org/10.1017/JMECH.2014.72.

Ascione, F., Servi, C.M.D., Meijer, O., Pommé, V., Colonna, P., 2021. Assessment of an inverse organic rankine cycle system for the ECS of a large rotorcraft adopting a high-speed centrifugal compressor and a low GWP refrigerant. In: Proceedings of the 6th International Seminar on ORC Power Systems. Technical University of Munich, http://dx.doi.org/10.14459/2021mp1633127.

Audet, C., Le Digabel, S., Rochon Montplaisir, V., Tribes, C., 2021. NOMAD version 4: Nonlinear optimization with the MADS algorithm. Technical report, Les cahiers du GERAD.

Audet, C., Le Digabel, S., Tribes, C., 2019. The mesh adaptive direct search algorithm for granular and discrete variables. 29, (2), pp. 1164–1189. http://dx.doi.org/10.1137/18M1175872.

Bender, D., 2018. Exergy-based analysis of aircraft environmental control systems and its integration into model-based design (Ph.D. thesis). http://dx.doi.org/10.14279/DEPOSITONCE-8101.

Blank, J., Deb, K., 2020. Pymoo: Multi-objective optimization in python. IEEE Access 8, 89497–89509. http://dx.doi.org/10.1109/ACCESS.2020.2990567.

Boeing, 2007. AERO, 4th quarter.

Cavallini, A., Censi, G., Del Col, D., Doretti, L., Longo, G., Rossetto, L., 2001. Experimental investigation on condensation heat transfer and pressure drop of new HFC refrigerants (R134a, R125, R32, R410A, R236ea) in a horizontal smooth tube. Int. J. Refrig. 24 (1), 73–87. http://dx.doi.org/10.1016/S0140-7007(00)00070-0.

Chang, Y.-J., Wang, C.-C., 1997. A generalized heat transfer correlation for Iouver fin geometry. Int. J. Heat Mass Transfer 40 (3), 533–544. http://dx.doi.org/10.1016/0017-9310(96)00116-0.

Colonna, P., Guardone, A., 2006. Molecular interpretation of nonclassical gas dynamics of dense vapors under the van der Waals model. Phys. Fluids 18 (5), 056101. http://dx.doi.org/10.1063/1.2196095.

Deb, K., Pratap, A., Agarwal, S., Meyarivan, T., 2002. A fast and elitist multiobjective genetic algorithm: NSGA-II. IEEE Trans. Evol. Comput. 6 (2), 182–197. http://dx.doi.org/10.1109/4235.996017.

Dechow, M., Nurcombe, C., 2005. Aircraft environmental control systems. In: Hocking, M. (Ed.), Air Quality in Airplane Cabins and Similar Enclosed Spaces. Springer Berlin Heidelberg, Berlin, Heidelberg, pp. 3–24. http://dx.doi.org/10.1007/b107234.

Duan, Z., Sun, H., Wu, C., Hu, H., 2022. Multi-objective optimization of the aircraft environment control system based on component-level parameter decomposition. Energy 245, 123330. http://dx.doi.org/10.1016/J.ENERGY.2022.123330.

Eckardt, D., 1975. Instantaneous measurements in the jet-wake discharge flow of a centrifugal compressor impeller. J. Eng. Gas Turbines Power 97 (3), 337–345. http://dx.doi.org/10.1115/1.3445999.

Eckardt, D., 1976. Detailed flow investigations within a high-speed centrifugal compressor impeller. J. Fluids Eng. Trans. ASME 98 (3), 390–399. http://dx.doi.org/10.1115/1.3448334.

Eckardt, D., 1977. Doctoral Dissertation. Technical report, pp. 1–227.

Giuffre, A., Colonna, P., Pini, M., 2022. The effect of size and working fluid on the multi-objective design of high-speed centrifugal compressors. Int. J. Refrig. 143, 43–56. http://dx.doi.org/10.1016/J.IJREFRIG.2022.06.023.

Giuffre', A., Colonna, P., Pini, M., 2023. Design optimization of a high-speed twin-stage compressor for next-gen aircraft environmental control system. J. Eng. Gas Turbines Power 145 (3), http://dx.doi.org/10.1115/1.4056022.

Gnielinski, V., 2013. On heat transfer in tubes. Int. J. Heat Mass Transfer 63, 134–140. http://dx.doi.org/10.1016/j.ijheatmasstransfer.2013.04.015.

Japikse, D., 1987. A critical evaluation of three centrifugal compressors with pedigree data sets: Part 5-studies in component performance. J. Turbomach. 109 (1), 1–9. http://dx.doi.org/10.1115/1.3262064.

Kandlikar, S.G., 1990. A general correlation for saturated two-phase flow boiling heat transfer inside horizontal and vertical tubes. J. Heat Transfer 112 (1), 219–228. http://dx.doi.org/10.1115/1.2910348.

Kim, M.-H., Bullard, C.W., 2002a. Air-side thermal hydraulic performance of multi-louvered fin aluminum heat exchangers. Int. J. Refrig. 25 (3), 390–400. http://dx.doi.org/10.1016/S0140-7007(01)00025-1.

Kim, M.H., Bullard, C.W., 2002b. Performance evaluation of a window room air conditioner with microchannel condensers. J. Energy Resour. Technol. 124 (1), 47–55. http://dx.doi.org/10.1115/1.1446072.

Kouremenos, D.A., Kakatsios, X.K., 1985. The three isentropic exponents of dry steam. Forschung Im Ingenieurwesen 51 (4), 117–122. http://dx.doi.org/10.1007/BF02558416.

Kraft, D., 1988. A software package for sequential quadratic programming. Technical report, DLR German Aerospace Center – Institute for Flight Mechanics, Koln, Germany.

Leo, T.J., Pérez-Grande, I., 2005. A thermoeconomic analysis of a commercial aircraft environmental control system. Appl. Therm. Eng. 25 (2–3), 309–325. http://dx.doi.org/10.1016/J.APPLTHERMALENG.2004.06.011.

Li, X., Chen, Q., Hao, J.H., Chen, X., He, K.L., 2019. Heat current method for analysis and optimization of a refrigeration system for aircraft environmental control system. Int. J. Refrig. 106, 163–180. http://dx.doi.org/10.1016/J.IJREFRIG.2019.06.004.

Mounier, V., Picard, C., Schiffmann, J., 2018. Data-driven predesign tool for small-scale centrifugal compressor in refrigeration. J. Eng. Gas Turbines Power 140 (12), http://dx.doi.org/10.1115/1.4040845/457767.

Pangborn, H., Alleyne, A.G., Wu, N., 2015. A comparison between finite volume and switched moving boundary approaches for dynamic vapor compression system modeling. Int. J. Refrig. 53, 101–114. http://dx.doi.org/10.1016/J.IJREFRIG.2015.01.009.

Pérez-Grande, I., Leo, T.J., 2002. Optimization of a commercial aircraft environmental control system. Appl. Therm. Eng. 22 (17), 1885–1904. http://dx.doi.org/10.1016/S1359-4311(02)00130-8.

Rusch, D., Casey, M., 2013. The design space boundaries for high flow capacity centrifugal compressors. J. Turbomach. 135 (3), http://dx.doi.org/10.1115/1.4007548.

SAE, 2004. Aircraft fuel weight penalty due to air conditioning. http://dx.doi.org/10.4271/AIR1168/8.

Schiffmann, J., Favrat, D., 2009. Experimental investigation of a direct driven radial compressor for domestic heat pumps. Int. J. Refrig. 32 (8), 1918–1928. http://dx.doi.org/10.1016/j.ijrefrig.2009.07.006.

Schiffmann, J., Favrat, D., 2010. Design, experimental investigation and multi-objective optimization of a small-scale radial compressor for heat pump applications. Energy 35 (1), 436–450. http://dx.doi.org/10.1016/J.ENERGY.2009.10.010.

Schmidt, J., Friedel, L., 1997. Two-phase pressure drop across sudden contractions in duct areas. Int. J. Multiph. Flow. 23 (2), 283–299. http://dx.doi.org/10.1016/S0301-9322(96)00056-0.

Schmidt, S.A., Riedel, J., Hepcke, F., Casas, W., Bonhora, J., Lavergne, D., Sanchez, F., Ricard, G., 2021. New air systems for more electric aircraft. In: MEA2021, more Electric Aircraft - Towards Cleaner Aviation. Bordeaux, France.

Schweiger, G., Nilsson, H., Schoeggl, J., Birk, W., Posch, A., 2020. Modeling and simulation of large-scale systems: A systematic comparison of modeling paradigms. Appl. Math. Comput. 365, 124713. http://dx.doi.org/10.1016/J.AMC.2019.124713, arXiv:1909.00484.

Shah, M., 1979. A general correlation for heat transfer during film condensation inside pipes. Int. J. Heat Mass Transfer 22 (4), 547–556. http://dx.doi.org/10.1016/0017-9310(79)90058-9.

Shah, R.K., Sekulić, D.P., 2003. Fundamentals of Heat Exchanger Design. John Wiley & Sons, Ltd, Hoboken, NJ.

Sheikholeslami, M., Hatami, M., Jafaryar, M., Farkhadnia, F., Ganji, D.D., Gorji-Bandpy, M., 2015. Thermal management of double-pipe air to water heat exchanger. Energy Build. 88, 361–366. http://dx.doi.org/10.1016/j.enbuild.2014.11.076.

Sielemann, M., Giese, T., Oehler, B., Gräber, M., 2011. Optimization of an unconventional environmental control system architecture. SAE Int. J. Aerosp. 4 (2), 1263–1275. http://dx.doi.org/10.4271/2011-01-2691.

Stanitz, J., 1952. One-dimensional compressible flow in vaneless diffusers of radial-and mixed-flow centrifugal compressors, including effects of friction, heat transfer and area change. Technical report.

Tiainen, J., Jaatinen-Värri, A., Grönman, A., Sallinen, P., Honkatukia, J., Hartikainen, T., 2021. Validation of the axial thrust estimation method for radial turbomachines. Int. J. Rotating Mach. 2021, http://dx.doi.org/10.1155/2021/6669193.

Vargas, J.V., Bejan, A., 2001. Integrative thermodynamic optimization of the environmental control system of an aircraft. Int. J. Heat Mass Transfer 44 (20), 3907–3917. http://dx.doi.org/10.1016/S0017-9310(01)00033-3.

von Backström, T.W., 2006. A unified correlation for slip factor in centrifugal impellers. J. Turbomach. 128 (1), 1–10. http://dx.doi.org/10.1115/1.2101853.

Yadav, M.S., Giri, S.A., Momale, V.C., 2017. Sizing analysis of louvered fin flat tube compact heat exchanger by genetic algorithm. Appl. Therm. Eng. 125, 1426–1436. http://dx.doi.org/10.1016/j.applthermaleng.2017.07.119.

Yan, Y.-Y., Lin, T.-F., 1998. Evaporation heat transfer and pressure drop of refrigerant R-134a in a small pipe. Int. J. Heat Mass Transfer 41 (24), 4183–4194. http://dx.doi.org/10.1016/S0017-9310(98)00127-6.

Yang, H., Yang, C., 2020a. Application of scaling-endoreversible thermodynamic analysis model to aircraft environmental control system-methodology development. Int. J. Refrig. 112, 90–99. http://dx.doi.org/10.1016/J.IJREFRIG.2019.12.006.

Yang, H., Yang, C., 2020b. Derivation and comparison of thermodynamic characteristics of endoreversible aircraft environmental control systems. Appl. Therm. Eng. 180, 115811. http://dx.doi.org/10.1016/J.APPLTHERMALENG.2020.115811.